Applied Geochemistry 100 (2019) 169–180

Contents lists available at ScienceDirect

Applied Geochemistry

journal homepage: www.elsevier.com/locate/apgeochem

Reactive transport calculations to evaluate sulphide fluxes in the near-field of a SF/HLW repository in the Opalinus Clay

Marek Pekala[a,*], Paul Wersin[a], Veerle Cloet[b], Nikitas Diomidis[b]

[a] Rock-Water Interaction, Institute of Geological Sciences, University of Bern, Baltzerstrasse 1+3, 3012, Bern, Switzerland
[b] NAGRA, Hardstrasse 73, 5430, Wettingen, Switzerland

ARTICLE INFO

Keywords:
Radioactive waste disposal
Microbial sulphate reduction
Sulphide
Corrosion of copper canister coating
Reactive transport modelling

ABSTRACT

Radioactive waste is planned to be disposed in a deep geological repository in the Opalinus Clay (OPA) rock formation in Switzerland. Copper coating of the steel disposal canister is considered as an option to ensure complete waste containment for a period of 100'000 years. Sulphide is a potential corroding agent to copper. While background sulphide concentrations in the OPA are very low (ca. 10^{-11} mol/L), it cannot be ruled out that sulphide reducing bacteria (SRB) thriving at discrete locations within the engineered barrier system (EBS) of the repository could generate significantly higher dissolved sulphide concentrations. The aim of this study is to conservatively evaluate the potential for SRB to generate and sustain elevated sulphide concentrations in the repository near-field by considering specific geochemical bottle-necks, to quantify the maximum sulphide fluxes towards the canister, and to assess their potential to corrode the copper canister coating. To address these objectives reactive transport calculations are performed, and main conceptual and parametric uncertainties of the model are assessed.

1. Introduction

In Switzerland, all categories of radioactive waste including spent nuclear fuel (SF) and vitrified high-level waste (HLW) are planned to be disposed in repositories constructed in the Opalinus Clay (OPA). SF and HLW will be encased in canisters, emplaced into horizontal tunnels excavated in the rock, and backfilled with a clay-rich material (MX-80 bentonite). Details on the reference disposal concept can be found in Nagra (2002). One of the long-term requirements for the canister is to provide complete radionuclide containment over a minimum period of 1000 years (Patel et al., 2012). Nagra (the Swiss National Cooperative for the Disposal of Radioactive Waste) is currently exploring various options for canister materials, copper-coated steel being one possibility, which can significantly prolong the canister lifetime (Holdsworth et al., 2014).

Sulphide is a potential corroding agent to copper under anaerobic conditions. Sulphide transport through the repository's engineered barrier system (Wersin et al., 2014; Briggs et al., 2016, 2017) and its corrosive effect have been evaluated by various nuclear waste disposal organisations who consider copper as canister material (SKI, 1996; SKB, 2010; SSM, 2011; Wersin et al., 2014). In the pristine OPA dissolved sulphide concentrations are very low (ca. 10^{-11} mol/L), controlled by the dissolution of pyrite (Pearson et al., 2003; Mäder, 2009). After re-saturation with the OPA pore water, reducing redox conditions will set in throughout the repository's near-field (Wersin et al., 2003). At equilibrium with pyrite, dissolved sulphide concentrations in the bentonite backfill will also be low.

Sulphate (celestite in the OPA – Wersin et al., 2013, and gypsum in the MX-80 buffer – Kiviranta and Kumpulainen, 2011) will be present in the repository's near-field, and its reduction could generate sulphide. It is known that at temperatures below 100 °C sulphate cannot be reduced to sulphide at a measurable rate without microbial mediation (e.g. Krauskopf, 1979; Grauer, 1991). Bacteria are abundant in deep subsurface (Whitman et al., 1998; McMahon and Parnell, 2014), and can thrive in zones hydrologically disconnected from the surface environment (Lovley and Chapelle, 1995). Some microbial communities inhabiting the deep subsurface have been shown to reduce sulphate to sulphide (Pedersen, 1997). Sulphate Reducing Bacteria (SRB) may utilise a variety of electron donors (e.g. organic compounds or hydrogen dissolved in the pore water) to reduce sulphate (e.g. Liamleam and Annachhatre, 2007; Muyzer and Stams, 2008). In OPA, sulphate reduction by bacteria utilising hydrogen (Bagnoud et al., 2016) and dissolved organics (Wersin et al., 2011) as electron donors has been demonstrated *in situ* at the Mont Terri Underground Research Laboratory (URL) in Switzerland. In the excavation-damaged zone (EDZ) of the emplacement drift, porosity will be increased due to the excavation of

* Corresponding author.
E-mail address: marek.pekala@geo.unibe.ch (M. Pekala).

https://doi.org/10.1016/j.apgeochem.2018.11.006
Received 10 December 2017; Received in revised form 19 October 2018; Accepted 8 November 2018
Available online 14 November 2018
0883-2927/

the tunnel. Increased porosity and availability of an electron donor could trigger SRB activity, resulting in sulphate reduction to sulphide.

In this study, calculations are performed using the reactive transport (RT) methodology, which allows direct coupling of bio-geochemical reactions and mass transfer. A simplified 1D radial geometry of the near-field is considered, which allows material volumes to be accounted for. Therefore, the inventory of substrates for bio-geochemical reactions and dilution on diffusion are accurately represented. In view of significant conceptual and parametric uncertainties, realistic modelling of SRB activity near the repository, especially over long periods, is currently impossible. Therefore, an approach is adopted whereby uncertainties are bounded by a conservative choice of processes and parameter values, such that the estimated sulphide concentrations and fluxes are pessimistic.

The aims of this study are to: (1) conservatively assess the potential for SRB to generate elevated sulphide concentrations in the near-field by considering specific geochemical bottle-necks, (2) quantify main model uncertainties, and (3) to conservatively evaluate maximum sulphide fluxes towards the canister as well as (in a simplified manner) assess their potential to corrode the copper canister coating.

2. Conceptual model and assumptions

The conceptual model considers that sulphate minerals present in the backfill (gypsum, $CaSO_4{\cdot}2H_2O(s)$) and in the surrounding OPA (celestite, $SrSO_4(s)$) are the source of dissolved sulphate for SRB activity. The minerals can dissolve/precipitate according to:

$$CaSO_4{\cdot}\,2H_2O(s) \leftrightarrow Ca^{2+}(aq) + SO_4^{2-}(aq) + 2H_2O \quad (1)$$

$$SrSO_4(s) \leftrightarrow Sr^{2+}(aq) + SO_4^{2-}(aq) \quad (2)$$

Solid organic matter (SOM) is present both in the bentonite backfill and in the OPA. SOM can release dissolved organic matter (DOM) into the pore water according to:

$$SOM(s) \rightarrow DOM(aq) \quad (3)$$

SRB are assumed inactive in the undisturbed OPA (Stroes-Gascoyne et al., 2007) and in the highly compacted bentonite backfill (Pedersen et al., 2000; Masurat et al., 2010; Stroes-Gascoyne et al., 2010; Stone et al., 2016), but active in the excavation-damaged zone (EDZ) of the OPA, where small open fractures provide space for bacterial viability. SRB can utilise naturally occurring dissolved organic matter as electron donor and sulphate as electron acceptor in their metabolic activities. Sulphide generation is accompanied by the release of CO_2 (which causes acidification via the formation of carbonic acid) according to the reaction (where DOM is simplistically represented by $CH_2O(aq)$ to indicate reaction stoichiometry):

$$2CH_2O(aq) + SO_4^{2-}(aq) + H^+(aq) \rightarrow HS^-(aq) + 2H_2O + 2CO_2(aq) \quad (4)$$

The generated sulphide may partly precipitate in the EDZ due to solubility constraints, and partly diffuse out of the EDZ. It is assumed that a ferrous sulphide mineral with a 1:1 stoichiometry will be the most likely solubility-controlling phase according to:

$$Fe^{2+}(aq) + HS^-(aq) \leftrightarrow FeS(s) + H^+(aq) \quad (5)$$

Iron required for the precipitation of ferrous sulphide can be provided by the dissolution of siderite ($FeCO_3(s)$, in the OPA) and goethite (FeOOH(s), in the MX-80 backfill):

$$FeCO_3(s) + H^+(aq) \leftrightarrow Fe^{2+}(aq) + HCO_3^-(aq) \quad (6)$$

$$FeOOH(s) + 3H^+(aq) \leftrightarrow Fe^{3+}(aq) + 2H_2O \quad (7)$$

Other reactions in the geochemical model include: the dissolution/precipitation of calcite ($CaCO_3(s)$) and dolomite ($CaMgCO_3$), cation exchange for Na^+, Ca^{2+}, Mg^{2+} and K^+ (in the MX-80 backfill and in the OPA), and protonation/de-protonation reactions on montmorillonite surfaces (in the MX-80 backfill). The main geochemical reactions involved in sulphide cycling are schematically shown in Fig. 1.

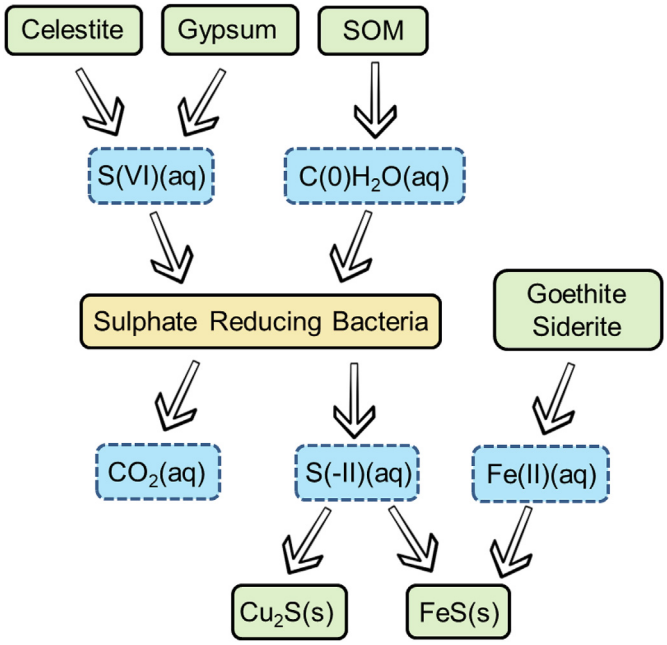

Fig. 1. Schematic of main processes considered in the conceptual geochemical model.

The rates of all mineral dissolution/precipitation reactions (except for SOM dissolution and sulphate reduction) are adjusted to mimic local chemical equilibrium. All aqueous reactions, exchange reactions and surface protonation reactions assume chemical equilibrium. Geochemical calculations are performed at 25 °C using the Thermochimie thermodynamic data base v.9b (Giffaut et al., 2014) utilising the Lawrence Livermore National Laboratory (LLNL) aqueous activity model.

S(VI) and S(-II) are the only redox states of sulphur considered in the model, while the S(VI)/S(-II) redox pair is decoupled from redox equilibrium. The microbial sulphate reduction reaction is represented as a kinetic Monod reaction of the form:

$$R_{SRB} = k_{SRB}\left(\frac{C_{DOM}}{C_{DOM} + K^s_{DOM}}\right)\left(\frac{C_{SO4}}{C_{SO4} + K^s_{SO4}}\right) \quad (8)$$

Where: R_{SRB} is the sulphate reduction rate [mol/(L_{water}·s)], k_{SRB} is the SRB activity rate constant [mol/(L_{water}·s)], C_{DOM} is the concentration of DOM [mol/L_{water}], K^S_{DOM} is the half-saturation constant for DOM [mol/L_{water}], C_{SO4} is the concentration of the sulphate species [mol/L_{water}], and K^S_{SO4} is the half-saturation constant for the sulphate species [mol/L_{water}]. Note that the simplified implementation of Monod kinetics represented by equation (8) assumes constant size of SRB population in time (k_{SRB} is a constant parameter).

The dissolution of SOM is represented as a kinetic reaction of the form:

$$R_{SOM} = k_{SOM}\left(1 - \frac{C_{DOM}}{C_{DOM,max}}\right) \quad (9)$$

Where R_{SOM} is the SOM dissolution rate [mol/(m^3_{bulk}·s)], k_{SOM} is the rate constant of SOM dissolution [mol/(m^3_{bulk}·s)], C_{DOM} is the DOM concentration [mol/L], and $C_{DOM,max}$ is the maximum DOM concentration [mol/L].

Copper canister corrosion is represented simplistically by assuming instantaneous sulphide consumption at the canister surface according to the stoichiometry: 2 mol of Cu consumed per 1 mol of sulphide. The

reaction stoichiometry additionally includes the consumption of protons, to mimic the formation of chalcopyrite according to:

$$2Cu(s) + HS^{-}(aq) + H^{+}(aq) \rightarrow Cu_2S(s) + H_2(aq) \quad (10)$$

Corrosion is controlled by the rate of sulphide transport towards the canister surface, and is therefore proportional to the time-integrated sulphide flux. The potential formation of solid corrosion products and their potential protective effects is disregarded, and uniform corrosion is considered. Furthermore, the impact of hydrogen generated by chalcocite precipitation is ignored.

Mass transfer is by diffusion in the water-filled porosity according to Fick's law, and considering an effective diffusion coefficient common to all dissolved species. Materials are represented as continuous porous compartments with homogenous properties, which are fully water-saturated and under isothermal conditions. It is further assumed that mineral dissolution and precipitation reactions have no impact on porosity and diffusivity, and the effect of increased temperature is neglected.

3. Input data

3.1. MX-80 backfill

Goethite content in the backfill is estimated at 0.64 wt % based on Fe mass balance using data of Kiviranta and Kumpulainen (2011). Solid organic matter is estimated at 0.1 wt.-% based on Wersin et al. (2014). The remaining mineralogical composition of the backfill is simplified after Kiviranta and Kumpulainen (2011) to include: montmorillonite (only for surface protonation and ion exchange reactions), gypsum, calcite and quartz. For cation exchange and surface protonation in the MX-80 backfill the models and parameterisation of Bradbury and Baeyens (2003), and Bradbury and Baeyens (1997), respectively, are used. The total porosity of the bentonite backfill is 0.48 (Van Loon, 2014), dry density equals 1'450 kg/m^3 (Savage, 2014), and the effective diffusion coefficient is $2{\cdot}10^{-12}$ m^2/s (Nagra, 2014b).

3.2. OPA and EDZ

Solid organic matter is taken to be present at 0.6 wt % (Nagra, 2014a). The remaining mineralogical composition of the OPA was simplified after Nagra (2014a) to include: calcite, siderite, dolomite and quartz. Celestite is estimated based on Wersin et al. (2013). A generic exchanger is implemented to represent cation exchange reactions with total CEC and composition reported by Pearson (2002). The total porosity is 0.11 (Gaus et al., 2014) and 0.14 (Nagra, 2014a) for the OPA and the EDZ, respectively. The effective diffusion coefficient equals $2{\cdot}10^{-12}$ m^2/s and 10^{-11} m^2/s for the OPA and the EDZ, respectively (Nagra, 2014b).

Diffusive transport in the OPA and in the MX-80 backfill is treated simplistically by considering a single porosity and a common effective diffusion coefficient (D_e) to all dissolved species, with a value characteristic of anions. The choice of D_e characteristic of anions is justified by the expectation that sulphate transport will be predominantly in the anionic form (SO_4^{2-}(aq)), and so will be the sulphide (HS^-(aq)) generated by SRB. It is recognized however, that solute transport in compacted clays is complex: anions, cations and neutral species are affected differently, and that there remain uncertainties regarding the overall effect on sulphide generation and transport.

3.3. Key parametric uncertainties

Mathematical representation of the conceptual model described above requires that a number of parameter values be quantified. Some of these values are poorly constrained under disposal conditions. Below, key areas of uncertainty are identified, and parameter values are estimated based on available laboratory and field data.

3.4. Rate of SRB activity

The maximum rate of SRB activity (at full substrate availability) is defined according to equation (8) by the rate constant k_{SRB}. This lumped parameter represents the intrinsic ability of SRB to reduce sulphate and the size of bacterial population (biomass). Rates of microbial sulphate reduction observed in nature and laboratory experiments vary by orders of magnitude (e.g. Goldhaber and Kaplan, 1975; Holmer and Starkholm, 2001; Wersin et al., 2011; Glombitza et al., 2013; Hallbeck, 2014; Glombitza et al., 2015; Richards and Pallud, 2016) with peak values around 1 mol/(L·yr), but usually significantly lower. Based on the above, the value of 0.1 mol/(L·yr) is assumed for the SRB rate constant (k_{SRB}). Additional sensitivity calculations are also carried out considering values of 1 and 10^{-5} mol/(L·yr). For the simplified Monod model (equation (8)), the DOM and sulphate half-saturation constants are defined at 10^{-6} mol/L, based on the review by Maia et al. (2016). This is similar to the values used by Grandia et al. (2006) for modelling of the Mont Terri *in situ* PC experiment ($3{\cdot}10^{-6}$ and 10^{-6} mol/L for acetate and sulphate half-saturation constants, respectively). Additional test calculation cases are performed assuming half-saturation constants of 10^{-9} and 10^{-3} mol/L.

3.5. Availability of DOM

DOM concentrations in anoxic extracts of the OPA were reported to be in the range 3.9 ± 0.4 to 8.8 ± 0.8 mg C/L (milligram carbon per litre solution), while DOM measured in the pore water were 1.2–15.8 ± 0.5 mg C/L (Courdouan Merz, 2008). Acetate, lactate and formate were identified in the extracts and pore water with LMWOA (low molecular weight organic acids) constituting 36% of the DOC. DOM concentration in the MX-80 bentonite is unknown. Based on the above, the DOC concentration ($C_{DOM,max}$ in Equation (9)) in both OPA and the MX-80 backfill is defined at 1 mg/L. Sensitivity calculation cases are additionally performed, where the DOC concentrations in OPA and the backfill are assumed to be 0.1 and 10 mg/L.

3.6. Rate of dissolution and extractability of SOM

Dissolution rates of SOM in the OPA and in the MX-80 bentonite are currently unknown. However, the dissolution of SOM found in soils has been studied, and the results are used here as a proxy to estimate two parameters: the rate of SOM dissolution and its extractability. Schaumann et al. (2000) evaluated the data presented by Reemtsma et al. (1999) and calculated the soil SOM dissolution rate of around 0.1 μg DOM per minute per g SOM. Assuming the atomic mass of 12 u (pure carbon) for DOM, dry density of OPA of 2'450 kg/m^3 and SOM content in the OPA of 0.6 wt% this corresponds to about $2{\cdot}10^{-6}$ mol/(m^3_{bulk}·s). Therefore, the value of 10^{-6} mol/(m^3_{bulk}·s) is adapted here as the upper limit for the rate of SOM dissolution in the OPA and the MX-80. A sensitivity calculation is additionally carried out by provisionally considering a value of 10^{-11} mol/(m^3_{bulk}·s) as the lower SOM dissolution rate. The total amount of organic matter in the OPA (Nagra, 2014a) and MX-80 bentonite (e.g. Karnland, 2010; Kiviranta and Kumpulainen, 2011) are known. As a limiting case, the entire reported content of SOM is assumed leachable. A sensitivity calculation is additionally carried out considering that only 1% of the total SOM present is leachable. This value is estimated based on leaching of SOM in OPA by Courdouan et al. (2007), and based on data on extractable DOC in MX-80 reported by Marshall et al. (2015).

3.7. The sulphide-solubility limiting mineral

Based on the widely studied chemistry of ferrous sulphide solutions (e.g. Rickard and Luther, 2007, and references therein) mackinawite (with logK = −3.6 for the reaction: Mackinawite (s) + H^+(aq) = Fe^{2+}(aq) + HS^-(aq) as implemented in the

Thermochimie thermodynamic database v.9.0b, Giffaut et al., 2014) is considered to be the sulphide solubility limiting mineral in most of the present calculations. In addition, to conservatively evaluate the upper limit of sulphide solubility, sensitivity calculations are performed by considering the amorphous FeS(am) (with logK = −2.95 for the reaction: $FeS(am) + H^+(aq) = Fe^{2+}(aq) + HS^-(aq)$ as implemented in the Thermochimie thermodynamic database v.9.0b, Giffaut et al., 2014) to be the sulphide solubility limiting mineral.

3.8. Iron availability

Siderite is reported as a constituent of the OPA, and is considered to control dissolved iron in the OPA pore water (Pearson et al., 2003; Mäder, 2009; Nagra, 2014a). However, there remain inconsistencies in assuming siderite equilibrium to model dissolved Fe concentrations measured in water samples collected at the Mont Terri URL in Switzerland (Pearson et al., 2003). This could be due to presence of a Fe-bearing solid solution. In most present calculations, siderite is assumed the solubility-controlling mineral for dissolved Fe. Furthermore, sensitivity calculations are carried out, where the solubility of siderite is arbitrarily decreased by a factor ten. This serves as a simplistic illustration of the impact of decreased iron availability.

3.9. Calculation cases

Based on the conceptual and parametric uncertainties discussed earlier, the calculation cases considered in this study are presented in Table 1.

3.10. Model set-up

3.10.1. Initial and boundary transport conditions

Initial geochemical conditions are presented in Table 2. The OPA pore water is calculated by assuming equilibrium with calcite, dolomite, quartz, celestite and siderite, and considering $CO_2(g)$ partial pressure of $10^{-2.2}$ bar. Fixed exchanger composition reported by Mäder (2009) is used to calculate the equilibrium concentration of Na^+, Mg^{2+}, K^+ and Sr^{2+}. It is assumed that the composition of the EDZ corresponds to that of the undisturbed OPA. The MX-80 backfill pore water is calculated by equilibrating the OPA pore water reported by Mäder (2009), assuming equilibrium with gypsum, calcite, quartz, goethite at partial pressure of $CO_2(g)$ equal $10^{-2.2}$ bar. Fixed cation exchanger reported by Bradbury and Baeyens (2003) is used to calculate the concentrations of Na^+, Mg^{2+}, K^+.

3.10.2. Geometry and numerical implementation

The calculations consider a 1D radial model domain (Fig. 2). The external transport boundary assumes constant OPA pore water composition (Table 2). Although the canister is included in the model geometry (to correctly represent dimensions and volumes), it is considered as chemically inert and diffusively impervious. Sulphide consumption at the canister surface is simplistically represented by defining an arbitrary small space (single cell of 1 cm length within the outer canister zone) for this reaction to take place in.

Calculations are carried out using PFLOTRAN (www.pflotran.org) with the Thermochimie thermodynamic database v.9.0b (Giffaut et al., 2014). Diffusive transport and chemical reactions are solved in a one-step global implicit manner. Aqueous complexation reactions, surface complexation and cation exchange reactions are implemented as equilibrium reactions. Mineral dissolution reactions are kinetic, but their rates are adjusted relative to transport rates such that local equilibrium is approximated.

Microbial reactions and SOM dissolution are implemented as kinetic reactions. Most calculations are performed for a period of 100'000 years. For selected calculation cases evolution during 1'000'000 years is considered. The backfill and EDZ are discretized with 1 cm cells, while the cell size in the OPA gradually increases from 1 cm at its contact with the EDZ to a maximum of 50 cm (10 m away from the EDZ).

Table 1
Calculation cases. Bold face indicates parameters of interest for a given case. †siderite solubility is reduced by a factor of ten.

Case code	SOM dissolution rate constant (k_{SOM}) [mol/(m_{bulk}^3·s)]	Maximum DOM concentration ($C_{DOM,max}$) [mg/L_{water}]	Extractable SOM [% of total]	Sulphide solubility controlling mineral	Iron solubility controlling mineral	SRB activity rate constant (k_{SRB}) [mol/(L_{water}·yr)]	Half-saturation constants (K^S_{DOM}, K^S_{SO4}) [mol/L_{water}]
REF1	**10^{-11}**	1	100	Mackinawite	Siderite	0.1	10^{-6}
REF2	**10^{-6}**	1	100	Mackinawite	Siderite	0.1	10^{-6}
DOM1a	10^{-11}	**0.1**	100	Mackinawite	Siderite	0.1	10^{-6}
DOM1b	10^{-11}	**10**	100	Mackinawite	Siderite	0.1	10^{-6}
DOM2a	10^{-6}	**0.1**	100	Mackinawite	Siderite	0.1	10^{-6}
DOM2b	10^{-6}	**10**	100	Mackinawite	Siderite	0.1	10^{-6}
EXT1	10^{-11}	1	**1**	Mackinawite	Siderite	0.1	10^{-6}
EXT2	10^{-6}	1	**1**	Mackinawite	Siderite	0.1	10^{-6}
SSOL1	10^{-11}	1	100	**FeS(am)**	Siderite	0.1	10^{-6}
SSOL2	10^{-6}	1	100	**FeS(am)**	Siderite	0.1	10^{-6}
FESOL1	10^{-11}	1	100	Mackinawite	**†Siderite 10x less**	0.1	10^{-6}
FESOL2	10^{-6}	1	100	Mackinawite	**†Siderite 10x less**	0.1	10^{-6}
SRB1a	10^{-11}	1	100	Mackinawite	Siderite	**1**	10^{-6}
SRB1b	10^{-11}	1	100	Mackinawite	Siderite	**10^{-5}**	10^{-6}
SRB2a	10^{-6}	1	100	Mackinawite	Siderite	**1**	10^{-6}
SRB2b	10^{-6}	1	100	Mackinawite	Siderite	**10^{-5}**	10^{-6}
HS1a	10^{-11}	1	100	Mackinawite	Siderite	0.1	**10^{-3}**
HS1b	10^{-11}	1	100	Mackinawite	Siderite	0.1	**10^{-9}**
HS2a	10^{-6}	1	100	Mackinawite	Siderite	0.1	**10^{-3}**
HS2b	10^{-6}	1	100	Mackinawite	Siderite	0.1	**10^{-9}**
PES	**10^{-6}**	**10**	**100**	**FeS(am)**	**†Siderite 10x less**	**1**	**10^{-9}**

Table 2
Initial geochemical conditions in the OPA, EDZ and MX-80. (1) Fe concentration assuming siderite equilibrium. 10 times lower concentrations are assumed for cases FESOL, (2) Dissolved organic matter (DOM) is assumed to have the generic molecular formula of CH_2O. Alternative DOM concentrations assumed in cases DOM, (3) Solid organic matter (SOM) in the MX-80 backfill. 100 times lower SOM considered for case EXT, (4) Solid organic matter (SOM) in the OPA and EDZ. 100 times lower SOM considered for case EXT, (5) FeS(am) is assumed instead of mackinawite for cases SSOL, (†) Minerals initially absent, but allowed to form if over-saturated.

	OPA and EDZ	MX-80 backfill
pH	7.28	7.31
pe	−3.08	−3.24
Eh (mV)	−182	−191
Total dissolved [mol/L]		
Na	1.67E-01	3.26E-01
Mg	5.80E-03	8.07E-03
Ca	8.08E-03	1.18E-02
Sr	3.10E-04	3.21E-04
K	1.64E-03	1.56E-03
Fe	(1)4.63E-05	4.71E-05
Si	1.82E-04	1.82E-04
Cl	1.60E-01	1.60E-01
C(IV)	2.95E-03	3.43E-03
S(VI)	1.72E-02	1.02E-01
S(-II)	8.70E-10	8.66E-10
(2)DOM	8.33E-05	8.33E-05
Minerals [volume fraction]		
Calcite	1.23E-01	1.07E-03
Dolomite	5.50E-03	(†)0.00
Siderite	3.71E-02	(†)0.00
Celestite	3.70E-04	(†)0.00
Gypsum	(†)0.00	5.66E-03
Quartz	1.84E-01	2.73E-02
Goethite	(†)0.00	2.17E-03
(3)SOM_MX-80	0.00	1.21E-04
(4)SOM_OPA	1.23E-03	0.00
(5)Mackinawite/FeS(am)	(†)0.00	(†)0.00

4. Results

Main features of geochemical evolution are presented in Fig. 3 as radial profiles of sulphate, DOM and sulphide concentrations, and the rate of SRB activity at 1'000 and 50'000 years for cases REF1 and REF2 (the slower and faster rate of SOM dissolution, respectively). SRB activity at EDZ interfaces with the backfill and OPA is enhanced, where diffusive fluxes increase the availability of sulphate and DOM.

Sulphide concentrations generated by SRB activity at the EDZ are higher considering the faster SOM dissolution rate (REF2) than considering the slower SOM dissolution rate (REF 1). Furthermore, considering the slower SOM dissolution rate (REF1) SRB activity becomes limited by diffusive supply of DOM, while under higher rates of SOM dissolution the supply of sulphate is the limiting factor (compare Fig. 3a and c). Under sulphate-limited SRB activity (REF2), gypsum and celestite dissolve fast, leading to complete gypsum dissolution after ca. 2'000 years (not shown). Following that, dissolved sulphate in the backfill becomes rapidly depleted, and SRB activity continues only at the EDZ contact with the OPA, where celestite dissolution continuously provides sulphate. It is also to note that considering the slower SOM dissolution rate (REF1), the calculated time required for complete gypsum consumption in the backfill is significantly longer, about 12'000–13'000 years (not shown).

Sulphide generated by SRB activity at the interfaces precipitates as mackinawite (Fig. 4, top), while the required Fe is supplied by siderite dissolution (Fig. 4, bottom). SRB activity in the EDZ increases sulphide solubility under mackinawite equilibrium by generating CO_2 (according to Equation (4)), which drives pore water acidification due to dissociation of carbonic acid. Fig. 5 shows the evolution of pH and the concentration of total dissolved sulphide calculated during 1'000'000 years at the centre of the EDZ for REF1 and REF2. The figure shows that (1) faster rate of SOM dissolution leads to higher SRB activity rate and increased acidification, and (2) lower pH leads to elevated concentration of dissolved sulphide (via mackinawite solubility). Following the SRB-driven perturbation, pH is predicted to reach a near steady state after about 100'000 to 200'000 years. The pH value at the steady state is defined by a balance between the rate of SRB activity, the efficiency of chemical pH buffering, and the rate of diffusive transport. After SRB activity slows down due to complete sulphate consumption in the EDZ, a rebound of the pH is predicted over a period of up to 200'000 years. This process is controlled by a combination of diffusive transport and buffering by the carbonate system.

Fig. 6 shows that sulphide fluxes towards the canister are directly proportional to dissolved sulphide concentrations in the EDZ. Figs. 5 and 6 indicate that the period of rapid geochemical changes is limited

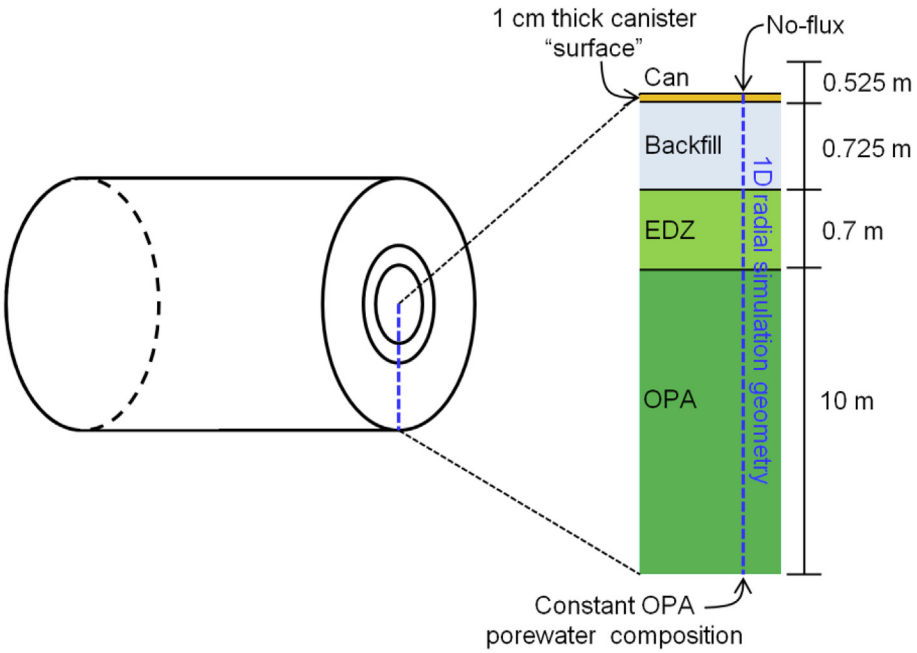

Fig. 2. Schematic illustration of the radial geometry of the disposal system with the orientation of 1D simulation profile used in reactive transport calculations (dashed blue line). Can – canister. Dimensions are not to scale. (For interpretation of the references to colour in this figure legend, the reader is referred to the Web version of this article.)

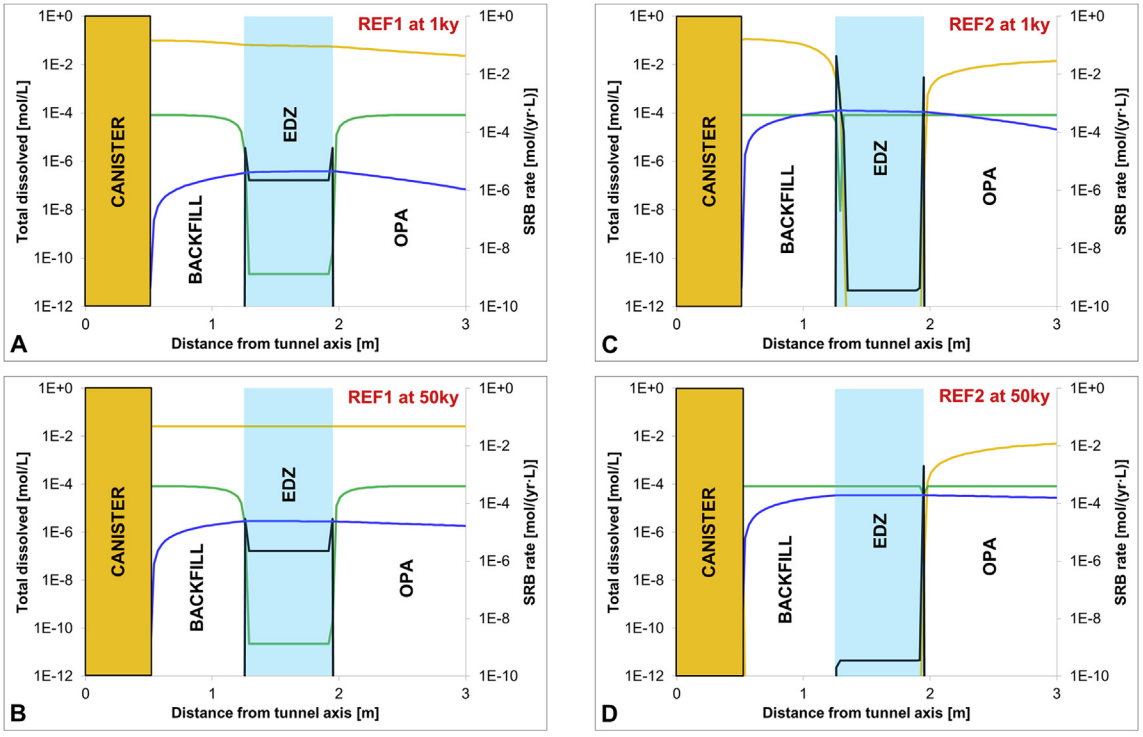

Fig. 3. Spatial profiles of total dissolved concentrations [mol/L] of sulphate (orange line), DOM (green line) and sulphide (blue line), and the rate of SRB activity [mol/(yr·L)] (black line) at 1'000 years (top) and 50'000 years (bottom) for REF1 (left) and REF2 (right). A) – REF1 at 1'000 years, B) – REF1 at 50'000 years, C) – REF2 at 1'000 years, and D) – REF2 at 50'000 years. (For interpretation of the references to colour in this figure legend, the reader is referred to the Web version of this article.)

to about 100'000 to 200'000 years. After this time, a near-steady state (at least in terms of sulphide fluxes towards the canister) is attained. Therefore, further discussions focus on the initial 100'000 years.

Fig. 7 (top) shows a comparison of sulphide fluxes towards the canister [mol/($m^2_{canister}$·yr)] predicted over a period of 100'000 years for all calculation cases. The calculated fluxes vary by a maximum of ca. four orders of magnitude. This is largely due to differences in the assumed rate of SOM dissolution. As discussed earlier, higher SOM dissolution rate leads to increased availability of DOM, enhanced SRB activity, stronger water acidification, and elevated sulphide concentrations due to mackinawite solubility.

The highest sensitivity is related with the sulphide- and iron-solubility controlling minerals. Considering FeS(am) (case SSOL) results in sulphide fluxes increasing by a factor of ca. 4.5 compared to assuming mackinawite as the sulphide-solubility controlling mineral. This reflects the ratio of the solubility constants of these two minerals ($K_{FeS(am)}/K_{mackinawite}$ = 4.5). Decreasing the solubility of the iron-controlling mineral by a factor of ten (FESOL), results in a sulphide flux decrease by a similar factor. The latter two observations are useful as they allow making simplified extrapolations of sulphide fluxes by considering various sulphide- and iron-controlling minerals. Moreover, a limited amount of extractable SOM (EXT1 and EXT2) leads to a significant decrease in sulphide fluxes due to limited availability of organics. On the other hand, the effect of varying DOM concentration within a range of 100 (DOM cases) has a small to negligible effect on the calculated flues (DOM2a and DOM2b are not shown as they overlap with REF2).

Varying the half-saturation constants within a range of six orders of magnitude (HS1a, HS1b, HS2a, HS2b – not shown) has practically no effect on the calculated sulphide fluxes. At the lower rate of SOM dissolution (SRB1a and SRB1b), varying the rate of SRB activity (increase 10 times or decrease 10'000 times) does not affect the sulphide flux to the canister (not shown). This suggests that sulphide flux is limited by availability of DOM and sulphate rather than by the capacity of SRB to utilise it. In the case of higher SOM dissolution rate (SRB2b), lowering the effective maximum SRB rate constant results in restricting the bacterial rate, and reduced sulphide fluxes to the canister. Fig. 7 (bottom) shows a comparison of the nominal canister corrosion depths calculated for selected cases over a period of 100'000 years. The total range of the calculated values at 100'000 years spans three orders of magnitude from $2{\cdot}10^{-6}$ to $2{\cdot}10^{-3}$ m. Table 3 presents a summary of the calculated nominal canister corrosion depths at 100'000 years, and the values calculated/estimated at 1'000'000 years.

Nominal canister corrosion depths at 1'000'000 years are calculated for the cases REF1, REF2 and PES. Based on the observation that a near-steady state in sulphide fluxes is developed after about 100'000 to 200'000 years, the corrosion depths at 1'000'000 years for other cases is estimated by linear extrapolation of the results at 100'000 years. Worth noting is that in cases for which corrosion depths at 1'000'000 years are calculated, the calculated values compare reasonably well with the estimated ones.

5. Discussion

Realistic predictive modelling of SRB activity near the repository over long times (hundreds of thousands of years and longer) is at present not possible due to its complexity and incomplete understanding of key processes. However, pessimistic estimates of sulphide concentrations and sulphide fluxes towards the canister can be derived from simplified models. For example, Briggs et al. (2017) presented 3D transport calculations of sulphide in the near field of the Canadian repository for Spent Fuel, where bio-geochemical reactions were represented implicitly using constant sulphide concentrations. In the present study, key reactions are represented explicitly using the reactive transport methodology. The advantage of this approach is that intrinsic coupling between reactions and diffusive transport are represented directly, and that the impact of certain geochemical bottlenecks is evaluated within a unified, dynamic geochemical framework. Uncertainties are bounded by a conservative choice of processes and

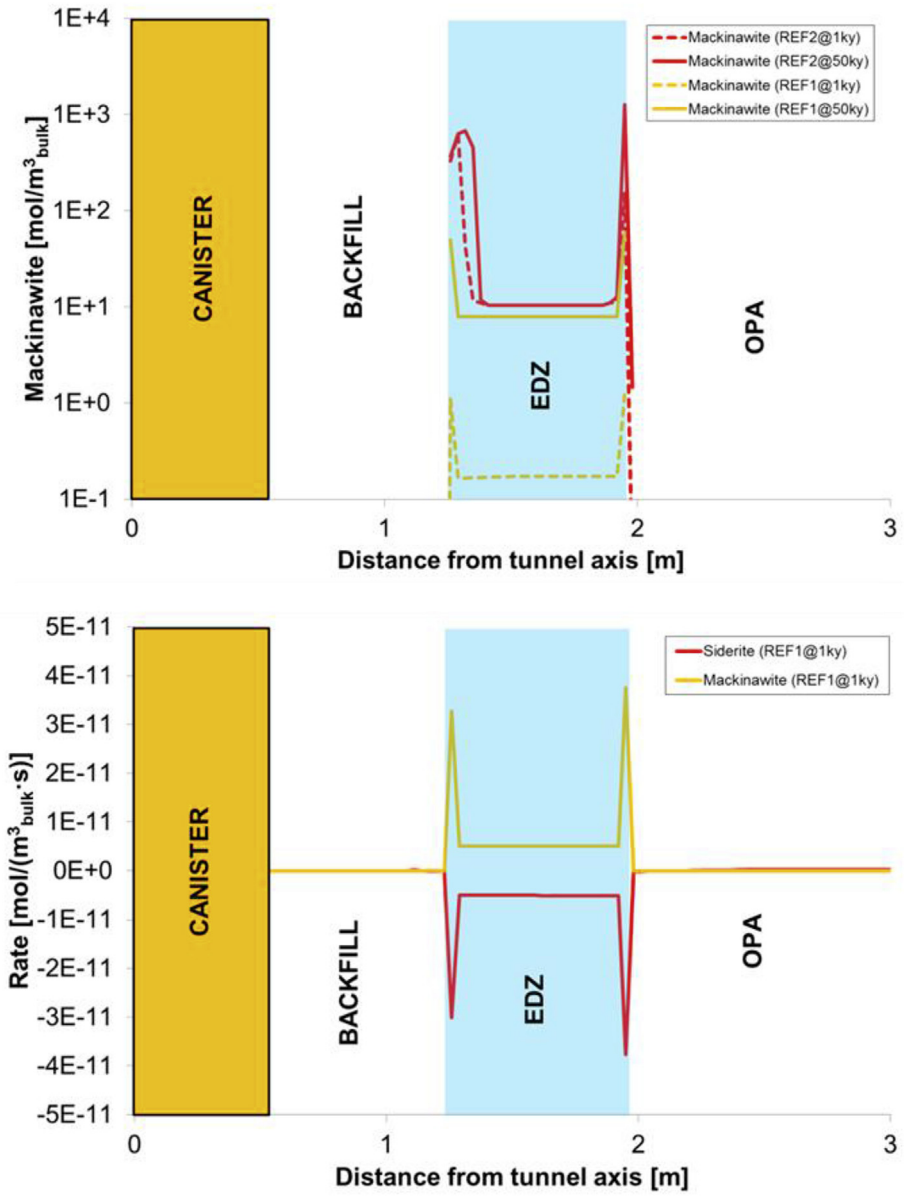

Fig. 4. Spatial profiles (radial distance from the tunnel centre) across the backfill, EDZ and OPA of mackinawite [mol/m^3_{bulk}] at two selected times (1'000 and 50'000 years) for cases REF1 and REF2 (top), and the dissolution/precipitation rates of siderite and mackinawite [mol/(m^3_{bulk}·s)] for the REF1 case at 1'000 years (bottom).

parameter values. Consequently, the predicted geochemical evolution does not aim to represent quantitatively the most likely geochemical evolution of the system. Instead, the choice of processes and parameter values results in a prediction of a geochemical evolution that is pessimistic in terms of sulphide concentrations and sulphide fluxes due to potential SRB activity. Modelling results and their limitations are discussed below.

Due to lack of relevant data for the OPA and the MX-80 bentonite, experimental results on SOM dissolution in soils (Reemtsma et al., 1999; Schaumann et al., 2000) are used to estimate the upper limit for this parameter at 10^{-6} mol/(m^3_{bulk}·s). Based on this assumption, the nominal corrosion depth at 1'000'000 years is calculated to be about $2{\cdot}10^{-4}$ m. It is noted however that this fast SOM dissolution rate value is likely an over-estimate as the "fresh" SOM found in recent soils is probably more soluble compared to the SOM in the OPA and in the MX-80 bentonite. In particular, the OPA is known to have undergone significant alterations during extended periods of heating and burial accompanying the diagenesis of the rock (Mazurek et al., 2006; Elie and Mazurek, 2008). Moreover, the experiments of Reemtsma et al. (1999) appear to have been carried out under atmospheric oxygen access. It is possible that (in comparison with oxygen depletion expected under disposal conditions) oxygen presence in the experiments leads to stronger SOM dissolution. Courdouan Merz (2008) reported noticeable increase in leachability of organic matter in the Callovo-Oxfordian with increasing exposure to oxygen. Recent work by Marshall et al. (2015) suggests that, due to a history of diagenetic alterations, SOM in the MX-80 bentonite is recalcitrant and poorly soluble. For example, water-extractable DOC (supposed to be representative of labile carbon in the pore water) in samples of MX-80 bentonite constitutes only about 8% of the total organic carbon. Likewise, Karnland (2010) suggests that the solid organic material in the MX-80 bentonite is "relatively insoluble". A realistic value for the SOM dissolution rate under relevant disposal conditions is currently impossible to quantify. Here an illustrative case is considered where the rate is arbitrarily reduced by 5 orders of magnitude to 10^{-11} mol/(m^3_{bulk}·s). Considering this lower SOM dissolution rate, the calculated nominal corrosion depth at 1'000'000 is about three times lower, $7{\cdot}10^{-5}$ m. For reasons similar to the ones discussed above, the extractable (soluble in the pore water) amount of

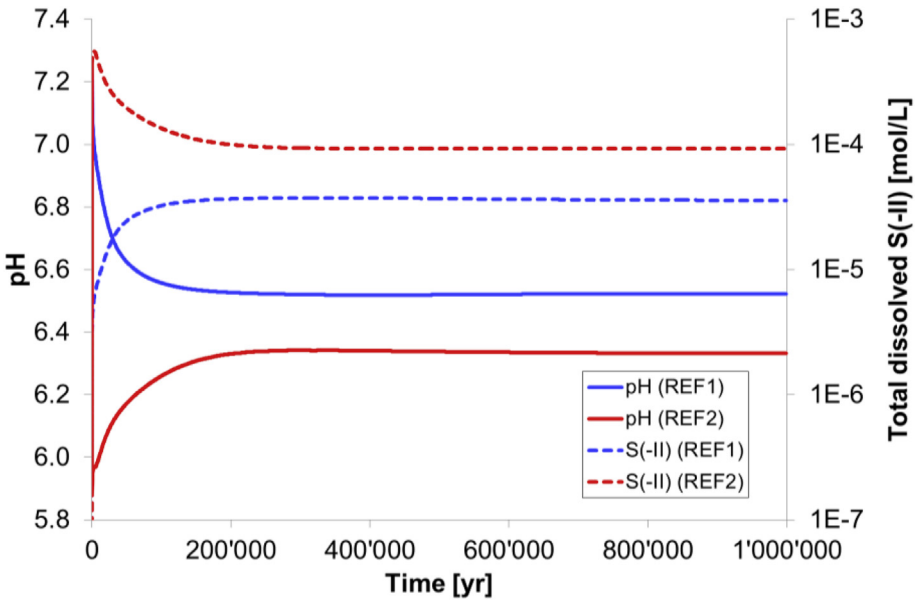

Fig. 5. pH and concentration of total dissolved sulphide (S(-II) [mol/L]) calculated during 1'000'000 years at the centre of the EDZ for calculation cases REF1 and REF2.

SOM likely constitutes only a small fraction of the total amount present. If the leachable amount of DOM in OPA reported by Courdouan et al. (2007) is considered (about 1%), the calculated corrosion depth is lower still, about $3{\cdot}10^{-5}$ m at 1'000'000 years, regardless of the SOM dissolution rate assumed. In the present model, DOM is represented using a simplified generic formula (CH_2O) for organic matter (Equation (4)), which implies a 2:1 carbon to sulphate reaction stoichiometry (e.g. sulphate reduction using acetate). It is noted that the reaction stoichiometry could be somewhat different depending on the actual composition of the reacting carbon specie. However, given the large pool of SOM present in the OPA, which is never exhausted in the calculation, this is a minor model uncertainty.

In the present model, the SRB capacity to reduce sulphate (including the size of the bacterial population) is included in the parameter k_{SRB} (Equation (8)), which defines the rate of SRB activity at full substrate availability. In the present calculations, the value of this parameter is conservatively estimated based on the maximum values observed in nature and in laboratory experiments. The calculations performed indicate that, while considering the slower SOM dissolution rate (lower DOM availability), varying the parameter had no appreciable effect on the calculated sulphide fluxes. This is interpreted to indicate that under such conditions, DOM availability limits sulphate reduction, not the capacity of SRB to do so. When the faster rate of SOM dissolution is considered (higher DOM availability), further increase in the k_{SRB} parameter has no effect on sulphide fluxes. This also indicates that the SRB capacity to reduce sulphate is not process limiting. However, while considering the faster rate of SOM dissolution, a reduction in k_{SRB} causes the fluxes to decrease, indicating that in such a case the capacity of SRB would limit the overall process of sulphate reduction. The above observations indicate that the assumed reference rate of SRB activity is high compared to DOM availability, even considering the upper limit on SOM dissolution rate. This is conservative as it assumes that the size of SRB population, and their intrinsic capacity to reduce sulphate, is not limiting for the calculated sulphide fluxes.

Uncertainties regarding iron and sulphide solubility in the EDZ may potentially have a significant impact. It is unlikely that amorphous FeS (am) should control dissolved sulphide in the EDZ for extended periods of time (e.g. hundreds of thousands of years). However, even considering such a case, the canister corrosion depth calculated at 1'000'000 years is pessimistically estimated at 1 mm. Worth noting is that mackinawite could convert to pyrite (e.g. Donald and Southam, 1999; Rickard and Morse, 2005; Rickard and Luther, 2007), especially in the long term. Given the very low solubility of pyrite under oxygen-free conditions, sulphide concentrations controlled by equilibrium with pyrite would be orders of magnitude lower.

As mentioned earlier, the current assumption is that siderite controls dissolved iron in the OPA pore water. Dissolved Fe concentrations measured in OPA are about ten times lower than the modelled ones assuming siderite equilibrium. This could be an artefact due to oxidation having taken place in the boreholes before sampling (Pearson et al., 2003). On the other hand, it cannot be ruled out, that the dissolved iron concentrations are representative of *in situ* conditions, which could be explained by equilibrium with a carbonate solid-solution that restricts iron solubility. A simplistic calculation considering the solubility of siderite arbitrarily decreased by a factor of ten leads to a maximum (for the faster SOM dissolution rate) canister corrosion depth of about 3 mm at 1'000'000 years.

The calculation case PES, represents a speculative case intended to test model extremes, where all model parameter values are selected to increase sulphide fluxes towards the canister. The resulting estimated nominal corrosion depth for this case is 6 mm at 1'000'000 years. This should be considered a highly pessimistic and unlikely scenario.

A general comment concerning all calculations, especially those considering the faster rate of SOM dissolution, is that the minimum pH values calculated due to SRB activity (ca. 5.9) are lower than measured experimental data. Wersin et al. (2011) reported pH values measured during the Porewater (PC) experiment in OPA at the Mont Terri Underground Research Laboratory. The minimum pH values measured were around 6.8 (with a reported 0.2 pH unit uncertainty). The significantly lower pH values predicted by the model considering fast SOM dissolution rates could indicate that SRB rates assumed are conservatively fast. Alternatively, the assumed pH-buffering model in OPA could be incomplete and overlook an additional pH-relevant reaction (such as the dissolution of clay minerals). However, the effect of the predicted low pH values is to increase the concentrations of dissolved sulphide under mackinawite equilibrium, and is therefore pessimistic.

Another general aspect concerning all presented calculations is that the activity of SRB over very long periods is unknown. In this study an assumption is made that SRB are present and active throughout the simulation (100'000 years up to 1'000'000 years). This assumption is conservative as the activity of SRB could additionally be limited by factors other than the availability of sulphate and DOM. For example,

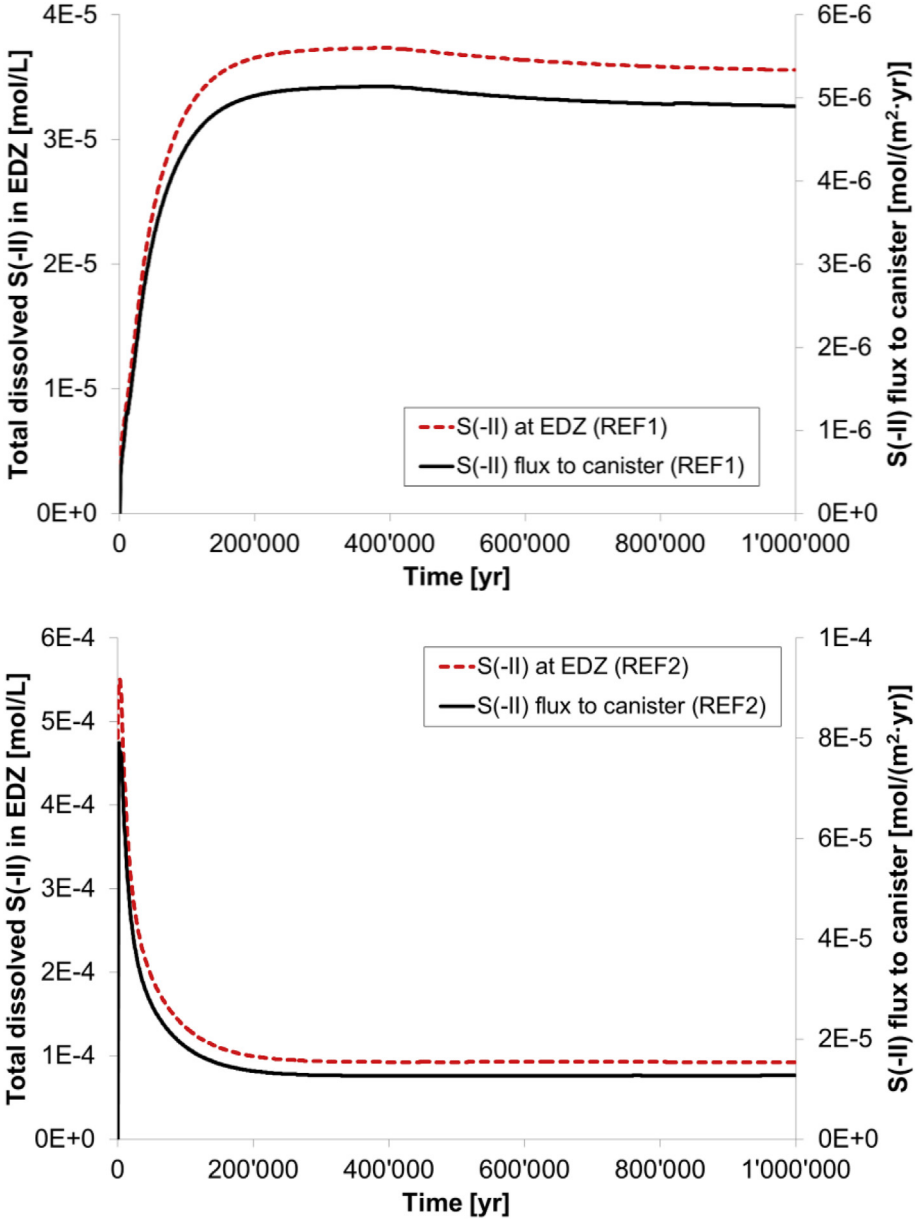

Fig. 6. Correlation of total dissolved sulphide concentration in the EDZ [mol/L] and sulphide fluxes towards the canister [mol/($m^2_{canister}$·yr)] over a period of 1'000'000 years for calculation cases REF1 (top) and REF2 (bottom).

microorganisms are dependent on the presence of trace elements, which constitute critical nutrients (such as Phosphorous). In the present model, it is conservatively assumed that such availability is never limiting for SRB.

The present geochemical model, and in particular the sulphide generation reaction, is largely de-coupled from redox. The sole potentially relevant redox coupling is via the iron system. However, under the model assumptions (initially reducing conditions in the pore water and redox buffering by the goethite/siderite mineral pair) redox remains reducing throughout the calculation, and importantly, dissolved iron remains almost completely dominated by Fe(II). As a result, redox has no practical effect on the modelled sulphide generation and sulphide fluxes. For this reason, the evolution of redox is not discussed further. It is to note however that relevant uncertainties concerning redox control in the OPA remain (Pearson et al., 2003; Mäder, 2009). The nature of the redox-controlling phases (sulphate/pyrite, goethite/siderite or magnetite/siderite) is not entirely clear, especially following a geochemical disturbance. Furthermore, the role of organic matter in microbial activity and redox reactivity of hydrogen generated by anaerobic corrosion of copper and steel is not fully understood (Wersin et al., 2003). Having in mind the above uncertainties, while decoupling the S(VI)/S(-II) redox pair equilibrium, potential sulphide oxidation due to a kinetic reaction was ignored. Likewise, potential sulphide oxidation to elemental sulphur was not accounted for. Both these simplifications are conservative in the sense that these additional potential sinks for sulphide are disregarded, although given the calculated pH and redox conditions (low dissolved oxygen concentrations) they are not expected to be significant.

6. Conclusions

In this study, the potential of SRB in the near-field of the repository for SF and HLW in the OPA in Switzerland is evaluated using the reactive transport methodology. In view of limited experimental information, a combination of conservative assumptions and data from analogue systems is used to estimate bounds on certain poorly

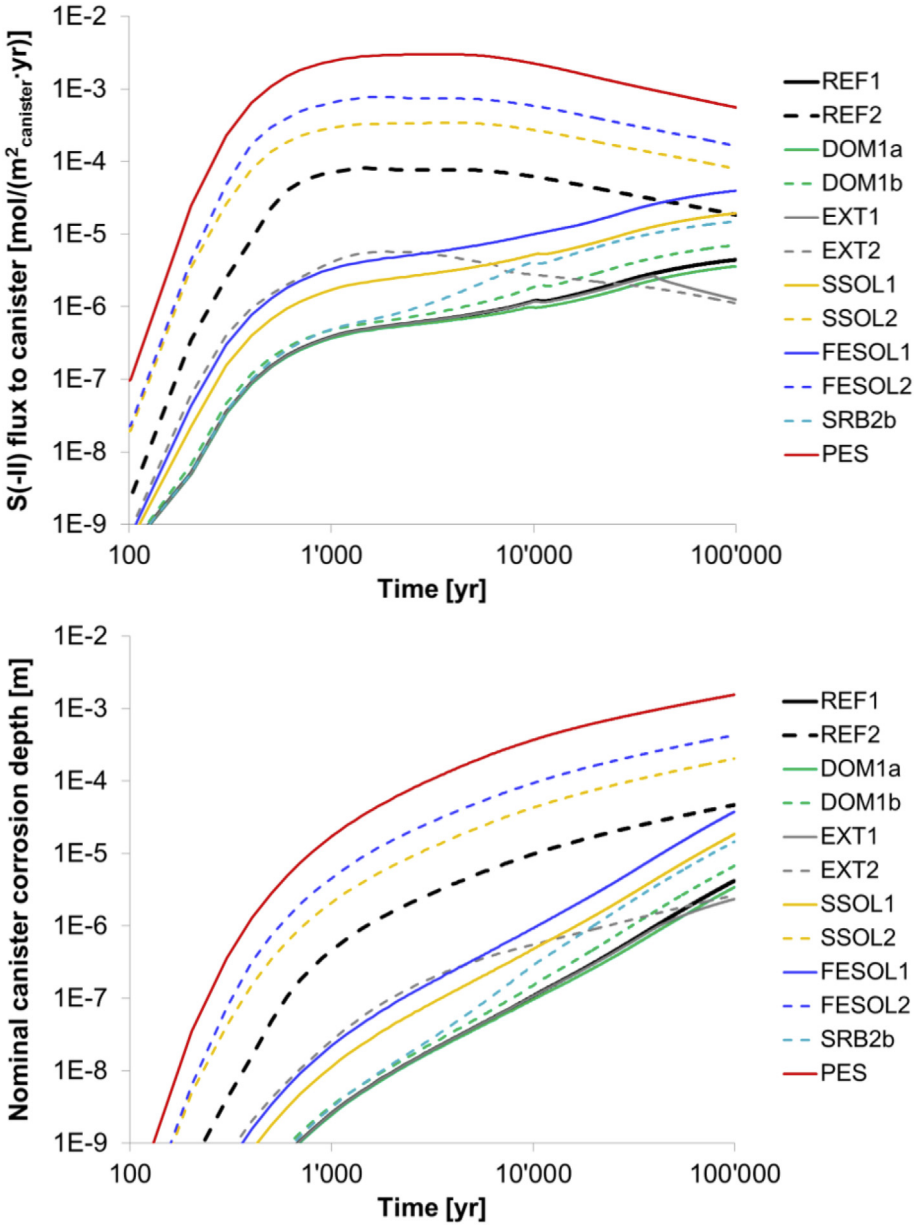

Fig. 7. Comparison of sulphide fluxes towards the canister [mol/($m^2_{canister}$·yr)] (top), and nominal canister corrosion depths [m] (bottom) calculated during 100'000 years for selected cases.

constrained model parameter values. The overall approach is to make assumptions that tend to enhance sulphide fluxes towards the canister, wherever conceptual or parametric uncertainties are encountered. In this sense, the calculated sulphide concentrations, sulphide fluxes towards the canister, and the estimated nominal corrosion depths are pessimistic.

Considering the conservative assumptions and model simplifications made, the results of this study suggest that SRB have the potential to generate dissolved sulphide concentrations significantly above the expected background values (approximately 10^{-11} mol/L, based on pyrite equilibrium). Given the large amount of sulphate and organic matter that could serve as electron donor to SRB in the OPA, sulphide generation could theoretically continue for a very long time (e.g. many hundreds of thousands of years). The assessment performed indicates that at 1'000'000 years the estimated nominal corrosion depth could be several millimetres in the most pessimistic cases considered. However, in view of the multiple conservative assumptions made, these values should be considered highly pessimistic. Nominal canister corrosion depths significantly below 1 mm at 1'000'000 years are more probable. Considering a copper coating thickness of about 3–5 mm, the results of this study suggest that sulphide-assisted copper corrosion is unlikely to compromise the copper coating during hundreds of thousands of years.

Outlook

In order to reduce the present level of conservatism in the model, further experimental and field data are indispensable. In particular, experimental data on *in situ* SRB activity (e.g. concentration of bacteria, selectivity towards specific organic compounds as electron donors, and availability of nutrients) under conditions comparable to those expected in the repository are needed. Moreover, experimental studies on the rate SOM dissolution in the OPA and the bentonite backfill under conditions relevant to disposal would be useful.

Additional issues are worthy further investigation, for example: electrostatic effects associated with ion transport in compacted clays, the effect of potential presence of cement and steel, SRB activity

Table 3
Summary of calculated nominal corrosion depths for all considered cases at 100'000 and 1'000'000 years. † – extrapolated from results obtained for 100'000 years.

Case code	Nominal corrosion depth at 100'000 years [m]	Nominal corrosion depth at 1'000'000 years [m]
REF1	$4{\cdot}10^{-6}$	$7{\cdot}10^{-5}$
REF2	$5{\cdot}10^{-5}$	$2{\cdot}10^{-4}$
DOM1a	$3{\cdot}10^{-6}$	†$5{\cdot}10^{-5}$
DOM1b	$7{\cdot}10^{-6}$	†$1{\cdot}10^{-4}$
DOM2a	$5{\cdot}10^{-5}$	†$3{\cdot}10^{-4}$
DOM2b	$5{\cdot}10^{-5}$	†$3{\cdot}10^{-4}$
EXT1	$2{\cdot}10^{-6}$	†$2{\cdot}10^{-5}$
EXT2	$3{\cdot}10^{-6}$	†$3{\cdot}10^{-5}$
SSOL1	$2{\cdot}10^{-5}$	†$3{\cdot}10^{-4}$
SSOL2	$2{\cdot}10^{-4}$	†$1{\cdot}10^{-3}$
FESOL1	$4{\cdot}10^{-5}$	†$5{\cdot}10^{-4}$
FESOL2	$4{\cdot}10^{-4}$	†$3{\cdot}10^{-3}$
SRB1a	$4{\cdot}10^{-6}$	†$6{\cdot}10^{-5}$
SRB1b	$4{\cdot}10^{-6}$	†$6{\cdot}10^{-5}$
SRB2a	$5{\cdot}10^{-5}$	†$3{\cdot}10^{-4}$
SRB2b	$1{\cdot}10^{-5}$	†$2{\cdot}10^{-4}$
HS1a	$4{\cdot}10^{-6}$	†$6{\cdot}10^{-5}$
HS1b	$4{\cdot}10^{-6}$	†$6{\cdot}10^{-5}$
HS2a	$5{\cdot}10^{-5}$	†$3{\cdot}10^{-4}$
HS2b	$5{\cdot}10^{-5}$	†$3{\cdot}10^{-4}$
PES	$2{\cdot}10^{-3}$	$6{\cdot}10^{-3}$

directly in the backfill in case of accidental poor emplacement, additional sulphide retardation effects (such as potential oxidation of sulphide to elemental sulphur or sulphate). These issues, as well as additional aspects, will be addressed in future work.

Acknowledgements

Financial support by Nagra is acknowledged. Peter Alt-Epping is thanked for helpful discussions. The authors are grateful to three anonymous reviewers for their comments.

References

Bagnoud, A., Chourey, K., Hettich, R.L., de Bruijn, I., Andersson, A.F., Leupin, O.X., Schwyn, B., Bernier-Latmani, R., 2016. Reconstructing a hydrogen-driven microbial metabolic network in Opalinus Clay rock. Nat. Commun. 7, 1–10.
Bradbury, M.H., Baeyens, B., 1997. A mechanistic description of Ni and Zn sorption on Na-montmorillonite Part II: modelling. J. Contam. Hydrol. 27, 223–248.
Bradbury, M.H., Baeyens, B., 2003. Porewater chemistry in compacted re-saturated MX-80 bentonite. J. Contam. Hydrol. 61, 329–338.
Briggs, S., McKelvie, J., Keech, P., Sleep, B., Krol, M., 2016. Transient modelling of sulphide diffusion under conditions typical of a deep geological repository. Corrosion Eng. Sci. Technol. 52 (Suppl. 1), 200–203.
Briggs, S., McKelvie, J., Sleep, B., Krol, M., 2017. Multi-dimensional transport modelling of corrosive agents through a bentonite buffer in a Canadian deep geological repository. Sci. Total Environ. 599–600, 348–354.
Courdouan, A., Christl, I., Meylan, S., Wersin, P., Kretzschmar, R., 2007. Isolation and characterization of dissolved organic matter from the Callovo–Oxfordian formation. Appl. Geochem. 22, 1537–1548.
Courdouan Merz, A., 2008. Nature and Reactivity of Dissolved Organic Matter in Clay Formations Evaluated for the Storage of Radioactive Waste. Unpublished PhD Thesis, ETH Zurich.
Donald, R., Southam, G., 1999. Low temperature anaerobic bacterial diagenesis of ferrous monosulfide to pyrite. Geochem. Cosmochim. Acta 63, 2019–2023.
Elie, M., Mazurek, M., 2008. Biomarker transformations as constraints for the depositional environment and for maximum temperatures during burial of Opalinus Clay and Posidonia Shale in northern Switzerland. Appl. Geochem. 23, 3337–3354.
Gaus, I., Garitte, B., Senger, R., Gens, A., Vasconcelos, R., Garcia-Sineriz, J.-L., Trick, T., Wieczorek, K., Czaikowski, O., Schuster, K., Mayor, J.C., Velasco, M., Kuhlmann, U., Villar, M.V., 2014. The HE-E Experiment: Lay-out, Interpretation and THM Modelling. Nagra Arbeitsbericht NAB 14–53 Nagra, Wettingen, Switzerland.
Giffaut, E., Grivé, M., Blanc, Ph, Vieillard, Ph, Colàs, E., Gailhanou, H., Gaboreau, S., Marty, N., Madé, B., Duro, L., 2014. Andra thermodynamic database for performance assessment: ThermoChimie. Appl. Geochem. 49, 225–236.
Glombitza, C., Stockhecke, M., Schubert, C., Vetter, A., Kallmeyer, J., 2013. Sulfate reduction controlled by organic matter availability in dee sediment cores from the saline, alkaline Lake Van (Eastern Anatolia, Turkey). Front. Microbiol. 4, 1–12.
Glombitza, C., Jaussi, M., Røy, H., Seidenkrantz, M.-S., Lomstein, B.A., Jørgensen, B.B., 2015. Formate, acetate and propionate as substrates for sulfate reduction sub-arctic sediments of Southwest Grenland. Front. Microbiol. 6, 1–14.
Goldhaber, M.B., Kaplan, I.R., 1975. Controls and consequences of sulfate reduction rates in recent marine sediments. Soil Sci. 119, 42–55.
Grandia, F., Domenech, C., Arcos, D., 2006. Porewater Chemistry (PC) Experiment: Results of the Geochemical Modeling. Technical Note, TN 2005-57, Mont Terri Project, St. Ursanne.
Grauer, R., 1991. The Reducibility of Sulphuric Acid and Sulphate in Aqueous Solution 109 Paul Scherrer Institute report.
Hallbeck, L., 2014. Determination of Sulphide Production Rates in Laboratory Cultures of the Sulphate Reducing Bacterium Desulfovibrio Aespoeensis with Lactate and H2 as Energy Sources. SKB Technical Report TR-14-14.
Holdsworth, S.R., Graule, T., Mazza, E., 2014. Feasibility Evaluation Study of Candidate Canister Solutions for the Disposal of Spent Nuclear Fuel and High Level Waste. A Status Review. Nagra Working Report. Nagra, Wettingen, Switzerland NAB 14-90.
Holmer, M., Storkholm, P., 2001. Sulphate reduction and sulphur cycling in lake sediments: a review. Freshw. Biol. 46, 431–451.
Karnland, 2010. Chemical and Mineralogical Characterization of the Bentonite Buffer for the Acceptance Control Procedure in a KBS-3 Repository. SKB Technical Report TR-10-60.
Kiviranta, L., Kumpulainen, S., 2011. Quality control and characterization of bentonite materials. Posiva 2011–2084 Working Report.
Krauskopf, K.B., 1979. Introduction to Geochemistry, second ed. McGraw & Hill, New York, pp. 617.
Liamleam, W., Annachhatre, A.P., 2007. Electron donors for biological sulfate reduction. Biotechnol. Adv. 25, 452–463.
Lovley, D.R., Chapelle, F.H., 1995. Deep subsurface microbial processes. Rev. Geophys. 33, 365–381.
Maia, F., Puigdomenech, I., Molinero, J., 2016. Modelling Rates of Bacterial Sulphide Production Using Lactate and Hydrogen as Energy Sources. SKB Technical Report TR-16-05.
McMahon, S., Parnell, J., 2014. Weighing the deep continental biosphere. FEMS Microbial Ecology 87, 113–120.
Marshall, M.H.M., McKelvie, J.R., Simpson, A.J., Simpson, M.J., 2015. Characterization of natural organic matter in bentonite clays for potential use in deep geological repositories for used nuclear fuel. Appl. Geochem. 54, 43–53.
Masurat, P., Eriksson, S., Pedersen, K., 2010. Microbial sulphide production in compacted Wyoming bentonite MX-80 under in situ conditions relevant to a repository for high-level radioactive waste. Appl. Clay Sci. 47, 58–64.
Mäder, U., 2009. Reference Porewater for the Opalinus Clay and "Brown Dogger" for the Provisional Safety-analysis in the Framework of the Sectoral Plan – Interim Results (SGT-ze). Nagra, Wettingen, Switzerland Arbeitsbericht NAB 09-14.
Mazurek, M., Hurford, A.J., Leu, W., 2006. Unravelling themulti-stage burial history of the Swiss Molasse Basin: integration of apatite fission track, vitrinite reflectance and biomarker isomerisation analysis. Basin Res. 18, 27–50.
Muyzer, G., Stams, A.J.M., 2008. The ecology and biotechnology of sulphate-reducing bacteria. Nat. Rev. Microbiol. 6, 441–454.
Nagra, 2002. Project Opalinus Clay. Nagra Technical Report, NTB 02-05. Nagra, Wettingen, Switzerland.
Nagra, 2014a. SGT Etappe 2: Vorschlag weiter zu untersuchender geologischer Standortgebiete mit zugehörigen Standortarealen für die Oberflächenanlage. In: Geologische Grundlagen: Dossier VI Barriereneigenschaften der Wirt- und Rahmengesteine. Nagra Technischer Bericht. 14–02 Nagra, Wettingen, Switzerland.
Nagra, 2014b. SGT Etappe 2: Vorschlag weiter zu untersuchender geologischer Standortgebiete mit zugehörigen Standortarealen für die Oberflächenanlage. In: Charakteristische Dosisintervalle und Unterlagen zur Bewertung der Barrierensysteme. Technischer Bericht. 14–03 Nagra, Wettingen, Switzerland.
Patel, R., Punshon, C.S., Nicholas, J., Bastid, P., Zhou, R., Schneider, C., Bagshaw, N., Howse, D., Hutchinson, E., Asano, R., King, F., 2012. Canister Design Concepts for Disposal of Spent Nuclear Fuel and High Level Waste 12–06 Nagra Technischer Bericht, NTB, Switzerland Nagra, Wettingen.
Pearson, F.J., 2002. Benken. Reference Water Chemistry. Unpublished Nagra Internal Report, Nagra, Wettingen, Switzerland.
Pearson, F.J., Arcos, D., Bath, A., Boisson, J.Y., Fernandez, A.M., Gaebler, H.E., Gaucher, E.C., Gautschi, A., Griffault, L., Hernan, P., Waber, H.N., 2003. Mont Terri Project - Geochemistry of Water in the Opalinus Clay Formation at the Mont Terri Rock Laboratory. Reports of the Federal Office of Water and Geology (FOWG). Geology Series No. 5.
Pedersen, K., 1997. Microbial life in deep granitic rock. FEMS (Fed. Eur. Microbiol. Soc.) Microbiol. Rev. 20, 399–414.
Pedersen, K., Motamedi, M., Karnland, O., Sandén, T., 2000. Mixing and sulphate-reducing activity of bacteria in swelling, compacted bentonite clay under high-level radioactive waste repository conditions. J. Appl. Microbiol. 89, 1038–1047.
Reemtsma, T., Bredow, A., Gehring, M., 1999. The nature and kinetics of organic matter release from soil by salt solution. Eur. J. Soil Sci. 50, 53–64.
Richards, C., Pallud, C., 2016. Kinetics of sulfate reduction and sulfide precipitation rates in sediments of a bar-built estuary (Pescadero, California). Water Res. 94, 86–102.
Rickard, D., Morse, J.W., 2005. Acid volatile sulfide (AVS). Mar. Chem. 97, 141–198.
Rickard, D., Luther III, G.W., 2007. Chemistry of iron sulphides. Chem. Rev. 107,

514–562.
Savage, D., 2014. An Assessment of the Impact of the Long Term Evolution of Engineered Structures on the Safety-relevant Functions of the Bentonite Buffer in a HLW Repository. Nagra, Wettingen, Switzerland Nagra Technical Report 13-02.
Schaumann, G.E., Siewert, Ch, Marschner, B., 2000. Kinetics of the release of dissolved organic matter (DOM) from air-dried and pre-moistened soil material. J. Plant Nutr. Soil Sci. 163, 1–5.
SKB, 2010. Corrosion Calculations Report for the Safety Assessment SR-site. SKB Technical Report TR-10-66.
SKI, 1996. CAMEO: a Model of Mass-Transport Limited General Corrosion of Copper Canisters. Swedish Nuclear Power Inspectorate. 96. pp. 46 SKI Report.
SSM, 2011. Is Copper Immune to Corrosion when in Contact with Water and Aqueous Solutions? Swedish Radiation Safety Authority. SSM Report 2011:09.
Stone, W., Kroukamp, O., McKelvie, J., Korber, D.R., Wolfaardt, G.M., 2016. Microbial metabolism in bentonite clay: saturation, desiccation and relative humidity. Appl. Clay Sci. 129, 54–64.
Stroes-Gascoyne, S., Schippers, A., Schwyn, B., Poulain, S., Sergeant, C., Simonoff, M., Le Marrec, C., Altmann, S., Nagaoka, T., Mauclaire, L., McKenzie, J., Daumas, S., Vinsot, A., Beaucaire, C., Matray, J.-M., 2007. Microbial community analysis of Opalinus clay drill core samples from the Mont Terri Underground Research laboratory, Switzerland. Geomicrobiol. J. 24, 1–17.
Stroes-Gascoyne, S., Hamon, C.J., Maak, P., Russell, S., 2010. The effects of the physical properties of highly compacted smectitic clay (bentonite) on the culturability of indigenous microorganisms. Appl. Clay Sci. 47, 155–162.
Van Loon, L.R., 2014. Effective Diffusion Coefficients and Porosity Values for Argillaceous Rocks and Bentonite: Measured and Estimated Values for the Provisional Safety Analyses for SGT-e2. Nagra, Wettingen, Switzerland Nagra Technical Report 12-03.
Wersin, P., Johnson, L.H., Schwyn, B., Berner, U., Curti, E., 2003. Redox Conditions in the Near Field of a Repository for SF/HLW and ILW in Opalinus Clay. Nagra, Wettingen, Switzerland Nagra Technical Report 02-13.
Wersin, P., Leupin, O.X., Mettler, S., Gaucher, E.C., Mäder, U., De Cannière, P., Vinsot, A., Gäbler, H.E., Kunimaro, T., Kiho, K., Eichinger, L., 2011. Biogeochemical processes in a clay formation in situ experiment: Part A – overview, experimental design and water data of an experiment in the Opalinus Clay at the Mont Terri Underground Research Laboratory, Switzerland. Appl. Geochem. 26, 931–953.
Wersin, P., Mazurek, M., Waber, H.N., Mäder, U., Gimmi, Th, Rufer, D., de Haler, A., 2013. Rock and Porewater Characterisation on Drillcores from the Schlattingen Borehole. Nagra Work Report NAB 12–54 Nagra, Wettingen, Switzerland.
Wersin, P., Alt-Epping, P., Pitkänen, P., Román-Ross, G., Trinchero, P., Molinero, J., Smith, P., Snellman, M., Filby, A., Kiczka, M., 2014. Sulphide Fluxes and Concentrations in the Spent Fuel Repository at Olkiluoto. Posiva Report 2014-01.
Whitman, B.W., Coleman, D.C., Wiebe, W.J., 1998. Prokaryotes: the unseen majority. Proceedings of National Academy of Sciences USA 95, 6578–6583.